Carbide evolution for a quenched and tempered Dievar steel

Yixin Xie[1], Shanshan Si[2], Yulin Ju[3]*, Rui Luo[1], Lei Zhou[3], Xiaonong Cheng[1,4]

1. School of Materials Science and Engineering, Jiangsu University, Zhenjiang, Jiangsu, China

2. Ansteel Beijing Research Institute Co. LTD., Beijing, China

3. Warwick Manufacturing Group, University of Warwick, Coventry, UK

4. Yangtze Delta Region Institute of Advanced Materials, Suzhou, Jiangsu, China

Abstract: Carbide precipitation, coarsening and hardness variations have been investigated for a quenched and tempered Dievar steel by SEM, TEM, STEM, HRTEM, XRD and hardness investigations. The carbide precipitation sequence has been ascertained as: M_8C_7 + bainitic / auto-tempered carbides $\rightarrow$ M_8C_7 + M_2C + M_7C_3 $\rightarrow$ M_8C_7 + M_7C_3 + $M_{23}C_6$ $\rightarrow$ M_8C_7 + M_7C_3 + $M_{23}C_6$ + M_6C. The boundary carbides coarsen significantly faster than the matrix ones. Hardness variations originating from the carbide evolution have been qualified. A fine-dispersion of M_2C carbides has led to a high hardness on tempering at 550 ℃, whereas the hardness drops drastically for tempering at 600 / 650 ℃ predominately due to the dissolution of unstable M_2C and the coarsening of carbides.

Keywords: Dievar steel, secondary alloy carbides, carbide coarsening, hardness evolution, secondary hardening

1. Introduction

Dievar is a new type of high-performance hot working die steel grade designed based on the chemical composition of H13 tool steel. It offers an excellent resistance to heat checking, gross cracking, hot wearing and plastic deformation at temperatures above 500 ℃, which has been widely used in the die casting-, forging- and extrusion industries[1]. The normal industrial heat treatment schedule for Dievar steel is spheroidizing annealing, austenization, oil quenching and high-temperature tempering, where the precipitation of secondary alloy carbides plays the main role in the strengthening of this grade of steel on tempering at temperatures $\geq$ 500 ℃[2].

The austenitizing temperature for hot working die steels has been reported in the temperature range of 1020 - 1080 ℃[3], where primary carbides have been observed after oil quenching. Hot working die steels after oil quenching at 1030 ℃ normally lead to a high hardness and good wear resistance, but a relatively lower impact toughness compared with samples quenching at other temperatures in the temperature range of 1020 - 1080 ℃[3, 4]. Undissolved primary carbides after quenching have been ascertained as V-rich MC carbides (or M_8C_7 - the substoichiometric composition of MC due to the carbon deficiency) due to its dissolution temperature being higher than the austenitizing temperature[5].

Many investigations have been carried out to study the precipitation of carbides for hot working die steels after different tempering schedules, where various sorts of secondary alloy carbides form with the diffusion of substitutional elements, such as Cr, Mo and V, which results in the variation in hardness values[5-7]. The equilibrium carbides in H13 steel tempered from 500 to 650 ℃ are MC, $M_{23}C_6$ combined with a small amount of M_6C according to thermodynamic simulations[8]. First of all, rod-like cementite has been detected in an H13MOD (Fe-0.38C-5.13Cr-1.84Mo-0.49V) steel on tempering at low temperatures; and coarsening of cementite occurs with the increase of tempering temperature, contributing to approximately 5 HRC hardness decrease for tempering at temperatures increasing from 540 ℃ to 600 ℃ for 2×2 h[5]. Secondly, needle-like Mo-rich M_2C carbides, exhibited to be coherent with the ferritic matrix, always precipitate after cementite and keep in very small sizes even at comparatively higher temperatures (e.g. >600 ℃), i.e. 0.28C-3Cr-2.9Mo-0.08Nb steel tempered at 640 ℃[9]. A higher Mo content in Dievar leads to a higher hardenability and a greater tempering resistance with a uniform distribution of Mo-rich M_2C carbides in the ferritic matrix responsible for the secondary hardening effect[2, 10, 11]. The decomposition from metastable M_2C carbides to M_6C carbides with a narrow thermodynamic stability region has also been reported to occur at tempering temperatures above 600 ℃[8]. The mass fraction of Mo-rich M_6C carbides is lower than that of Cr-rich M_7C_3 and $M_{23}C_6$ carbides due to its narrow thermodynamic

stability region[12]. Thirdly, Cr-rich M_7C_3 and $M_{23}C_6$ carbides with a polygonized or faceted structure have been found to form on tempering at around 600 ℃ and have a poor thermal stability, which is eager to coarsen or decompose, leading to the deterioration of strength and toughness[7, 13]. The precipitation of M_7C_3 carbides predominantly depends on the concentration of Cr atoms[14, 15], where Cr enriches cementite up to about 20 at.%[12], leaving only a small amount of Cr available in the solid solution of low Cr steels (less than ~3%[12]), resulting in the in-situ transformation from cementite to M_7C_3 particles. The formation of M_7C_3 and $M_{23}C_6$ takes place either via the *in-situ* transformation from alloyed cementite as Cr can take the place of iron atoms in cementite if there is sufficient soluble Cr in solid solution or by the separate nucleation in the ferritic matrix and along grain/sub-grain boundaries[16, 17]. Furthermore, there are two morphologies of V-rich MC / M_8C_7 carbides present on tempering at high temperatures for a longer time: larger and circular ones (primary carbides) and a fine dispersion of nano-sized ones derived from the transformation from other less thermal stable alloy carbides[5, 8, 9]. It has been shown that the uniform and fine dispersion of Mo-rich M_2C and V-rich MC/ M_8C_7 carbides in the ferritic matrix not only contributes to the secondary hardening but also confines the coarsening of martensitic laths, which further contributes to a higher tempering resistance in terms of maintaining high strength and excellent toughness for this grade of steel[18, 19].

A stable microstructure for Dievar steel at higher temperatures above 500 ℃ is desired, which is highly dependent on the research on the carbide formation and evolution during the quenching and tempering process. Several efforts on heat treatments and microstructure developments for this grade of steel have already been reported[20, 21]; however, the detailed carbide precipitation and coarsening behavior as well as their influences on the hardness variation have not been systematically and quantitatively studied. Therefore, the purpose of this paper is to investigate the carbide precipitation and evolution behavior for Dievar steel under various tempering time / temperature schedules; additionally, their contributions to the hardness

variation have been discussed as well. Eventually, the understanding of the carbide precipitation and hardness variation will significantly benefit the prediction of the tempering responses for these grades of steels.

2. Experimental Section

Dievar steel after vacuum smelting, electroslag and ultra-fine treatment was selected, and its chemical composition is shown in Table 1. Specimens with size of 130×40×30 mm were firstly isothermal spheroidizing annealed to produce an uniform structure with spherical carbides distributed in the ferrite. The spheroidizing annealed specimens were austenitized at 1030 ℃ for 0.5 h, followed by an oil quenching process. Finally, quenched samples were tempered at 550, 600 and 650 ℃ for 4 h, 8h, 16 h and 24 h.

Table 1. The chemical composition of Dievar steel (wt %)

Material	C	Mn	P	S	V	Mo	Cr	Si	Ni
Dievar	0.39	0.42	0.007	0.001	0.7	2.37	4.84	0.22	0.10

The microstructure evolution, mainly on the carbide precipitation and coarsening, was examined using a NovaNano450 scanning electron microscope (SEM), Jeol 2100 transmission electron microscope (TEM), Talos F200S scanning transmission electron microscope (STEM and HRTEM). SEM and bright-field (BF) images were used to observe the morphology of various carbides, while selected area diffraction patterns (SADP) were used to confirm the carbide types[5]. HRTEM was applied for the identification of needle-shaped carbides and the fourier transform method was used to determine and calibrate the carbide structure. High angle annular dark-field STEM (HAADF-STEM) imaging with energy dispersive X-ray spectroscopy (EDS) was utilized to ascertain carbide compositions in different tempering conditions. More than 100 carbides have been selected to confirm carbide types and compositions in each tempering condition. SEM samples with the size of 10×10×5 mm were polished

to a PO-S finish and etched in 4% natal for 30 s. Thin foil specimens for TEM and STEM observations were cut from the center of the as-quenched and tempered samples, then ground with mesh abrasive papers (grit no. 400-800-1000-2000) to 70 - 80 μm. Then, Gatan 695 ion beam thinner was used to produce a thin area by reducing the thinning voltage from 7 keV to 3 keV. Image J analysis software was used to obtain the length, width and distribution of particles from SEM or TEM images where approximately 1000 particles were measured for each assessed condition. An example showing the definition of carbide morphology categories on tempering is shown in Figure 1. Tiny needle-shaped carbides are present in the ferritic matrix. Larger spherical carbides and elliptical carbides with aspect ratio of 1.5 - 4 exist in the ferritic matrix and along boundaries. Carbides located at boundary are defined as boundary carbides, whereas carbides situated in the ferritic matrix are defined as matrix carbides.
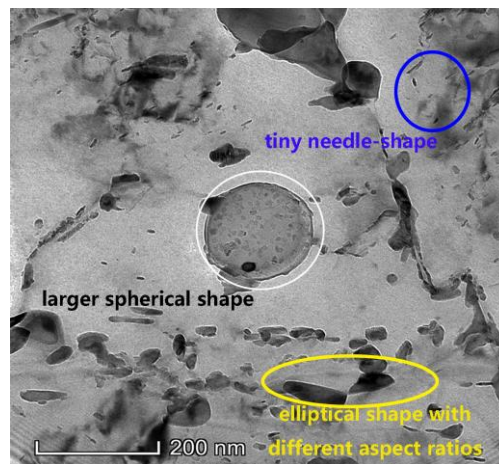

Figure 1. An example showing the definition of carbide morphology categories: tiny needle-shaped carbides in the matrix (blue circled), larger spherical carbides (white circled) and elliptical carbides (yellow circled).

XRD measurements were carried out using a X' Pert3 MRD instrument with a cobalt target (wavelength λ=1.78901 Å) to confirm the initial quenched microstructure for Dievar steel. XRD data were recorded in the 2θ range from 45° to 128°.

Rockwell macro-hardness (load 20 kg) testing[5] was used to measure sample hardness.

Fifteen indents were taken for each sample. Indents were taken at least 3 mm away from the sample edge to avoid the influence of the possible decarburization from the former heat treatment.

JMatPro with general steel database and Thermo-Calc software with TCFe 10 database[8] were employed to calculate carbide dissolution temperatures, equilibrium carbide volume fractions, equilibrium carbide compositions in Dievar steel.

3. Results

3.1 As-quenched microstructure

Lath martensite, a small amount of lenticular martensite, lower bainite, retained austenite, larger spherical carbides and auto-tempered carbides have all been observed after oil quenching, seen in Figure 2. Due to the relatively large sample size ($130 \times 40 \times 30$ mm) and the cooling rate estimated to be lower than 9 ℃/s[22] for the temperature region of 300 - 350 ℃ on oil quenching, lower bainite forms where cementite with the average length of 130 ± 20 nm precipitates as parallel arrays at about 60º to the axis of the bainitic plate, white arrowed in Figure 2 (a). Auto-tempering takes place within martensitic laths during oil quenching, where the average length for auto-tempered carbides is roughly 90 ± 20 nm, red arrowed in Figure 2 (b). Lenticular martensite, shown in Figure 2 (c), has been transformed from austenite on cooling, as the carbon content in the solid solution at 1030 ℃ is predicted to be 0.368 wt% (Thermo-Calc calculation) which supports the simultaneous formation of lath martensite and lenticular martensite. The XRD pattern of the oil-quenched sample is shown in Figure 2 (d), where the $(200)\gamma$ peak for the retained austenite is present. In terms of verifying the existence of the retained austenite in the as-quenched microstructure, the TEM observations using SADP and dark field images have been utilized in Figure 3. The retained austenite and spherical M_8C_7 carbides in this steel after oil quenching have both been ascertained. In addition, larger spherical carbides have been confirmed as V-rich M_8C_7 carbides with the diameter ranging from 100 to 300 nm, as shown in

Figure 3, which are considered as the undissolved primary carbides due to its dissolution temperature (theoretically calculated to be 1054 °C by Thermo-Calc) being higher than the austenitizing temperature 1030 °C[5, 6, 8]. Mo and Cr have been found to accumulate in these spherical V-rich M_8C_7 carbides.
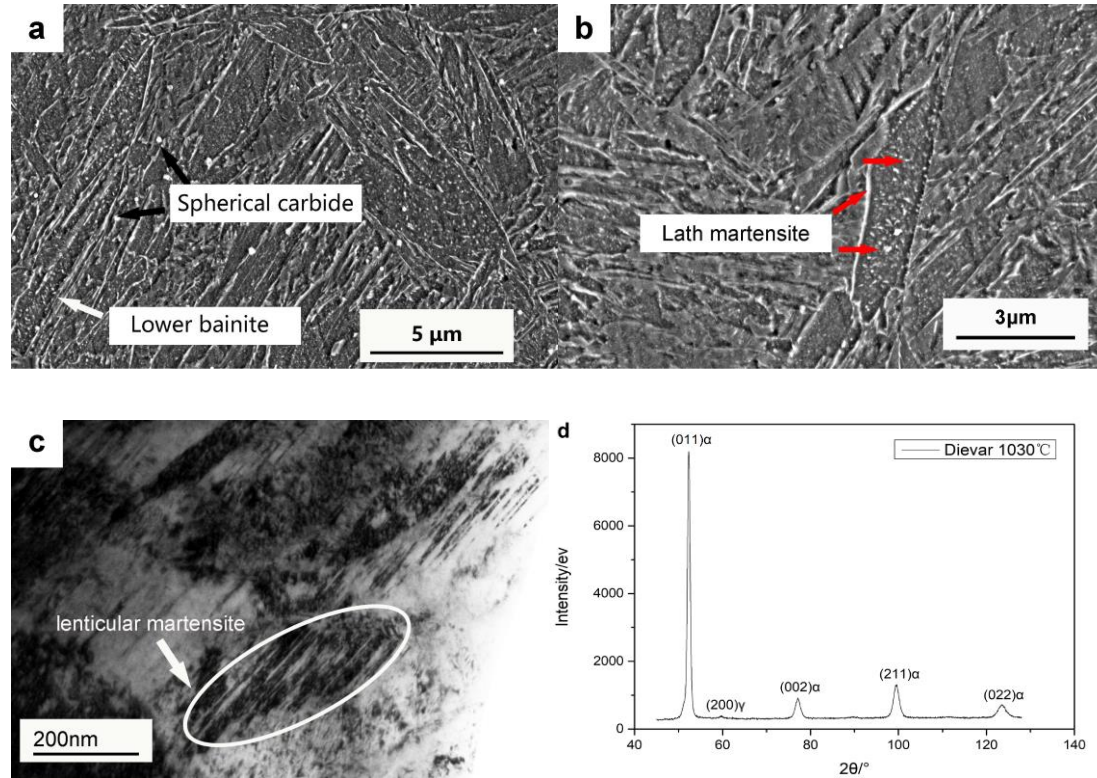

Figure 2. Microstructures of Dievar steel after oil quenching at 1030 °C: (a) (b) SEM images showing the presence of lath martensite (red arrowed), lower bainite (white arrowed), larger spherical carbides (black arrowed) and auto-tempered carbides within martensitic laths (red arrowed); (c) TEM image showing the existence of lenticular martensite (white arrowed); (d) XRD results showing the presence of the retained austenite.
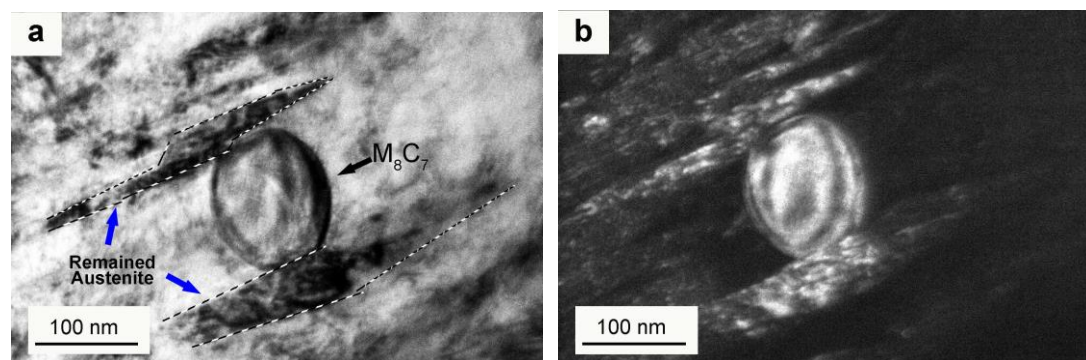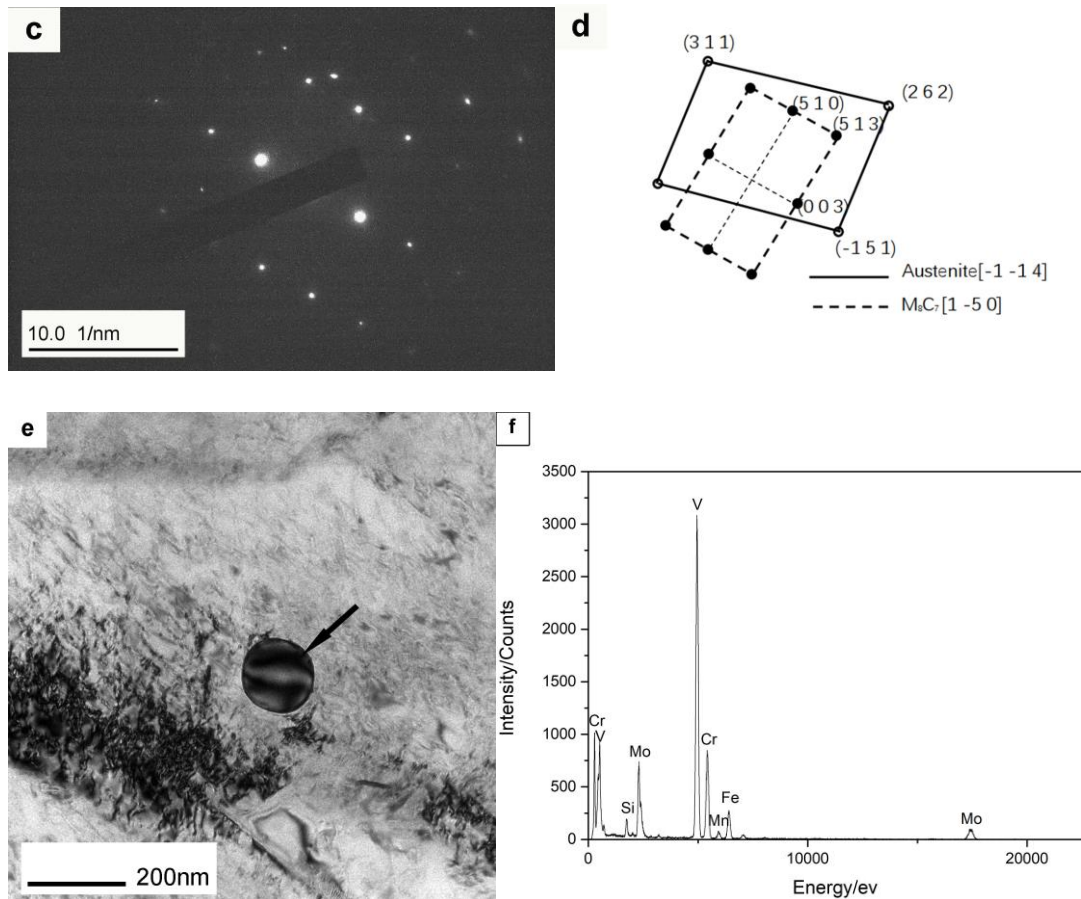
Figure 3. TEM images showing the presence of larger spherical carbides (black arrowed) and retained austenite (blue arrowed) after quenching at 1030 ℃ in Dievar steel: (a) (e) bright-field images; (b) Dark field pattern for (a); (c) (d) SAD pattern for (a); (f) EDS spectra for the particle in (e) (black arrowed).

3.2 Carbide precipitation and coarsening on tempering

As shown in Figure 4 and 5, different shapes of carbide are shown in SEM and TEM observations. Spherical carbides, elliptical carbides and very tiny needle-shaped carbides are present in different tempering stages. First of all, larger spherical carbides (white arrowed in Figure 4) persist at 550 - 650 ℃ for short and long tempering times. Secondly, very tiny needle-shaped carbides, black arrowed in Figure 5, have been observed within the matrix at lower temperatures even for a prolonged tempering procedure, like at 550 ℃ for 24 hours in Figure 5 (b). However, these carbides have disappeared with the increase of tempering temperatures, such as at 600 ℃ for 16 hours, Figure 5 (d). In addition, elliptical carbides preserve and coarsen at 550 - 650 ℃, yellow arrowed in Figure 4, which are probably either newly-formed alloy carbides or spheroidized pre-existing carbides.

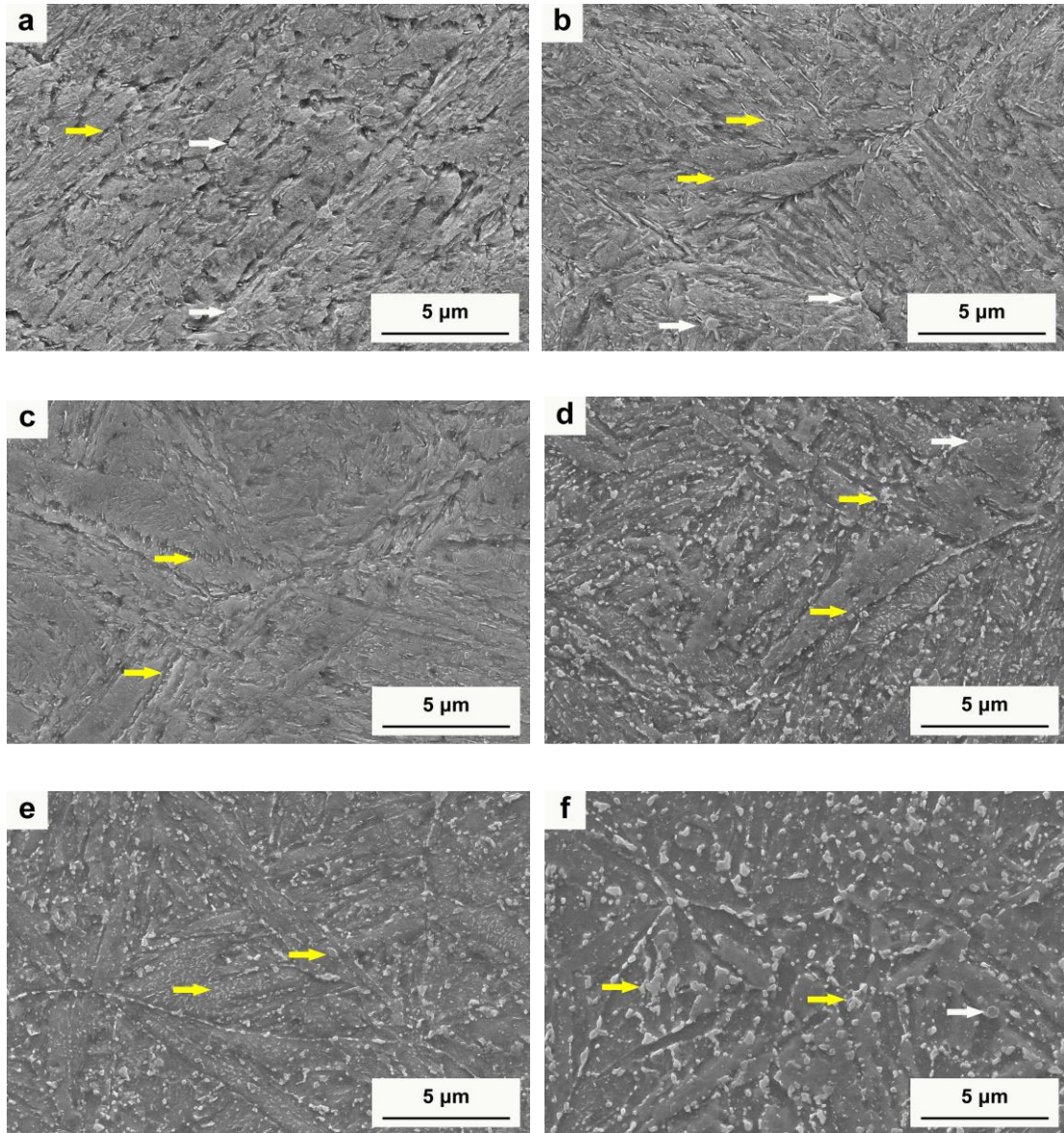Figure 4. Microstructures of Dievar steel after tempering at different temperatures for various time (SEM observations): (a) 550 ℃ for 4 h; (b) 550 ℃ for 24 h; (c) 600 ℃ for 4 h; (d) 600 ℃ for 24 h; (e) 650 ℃ for 4 h; (f) 650 ℃ for 24 h.
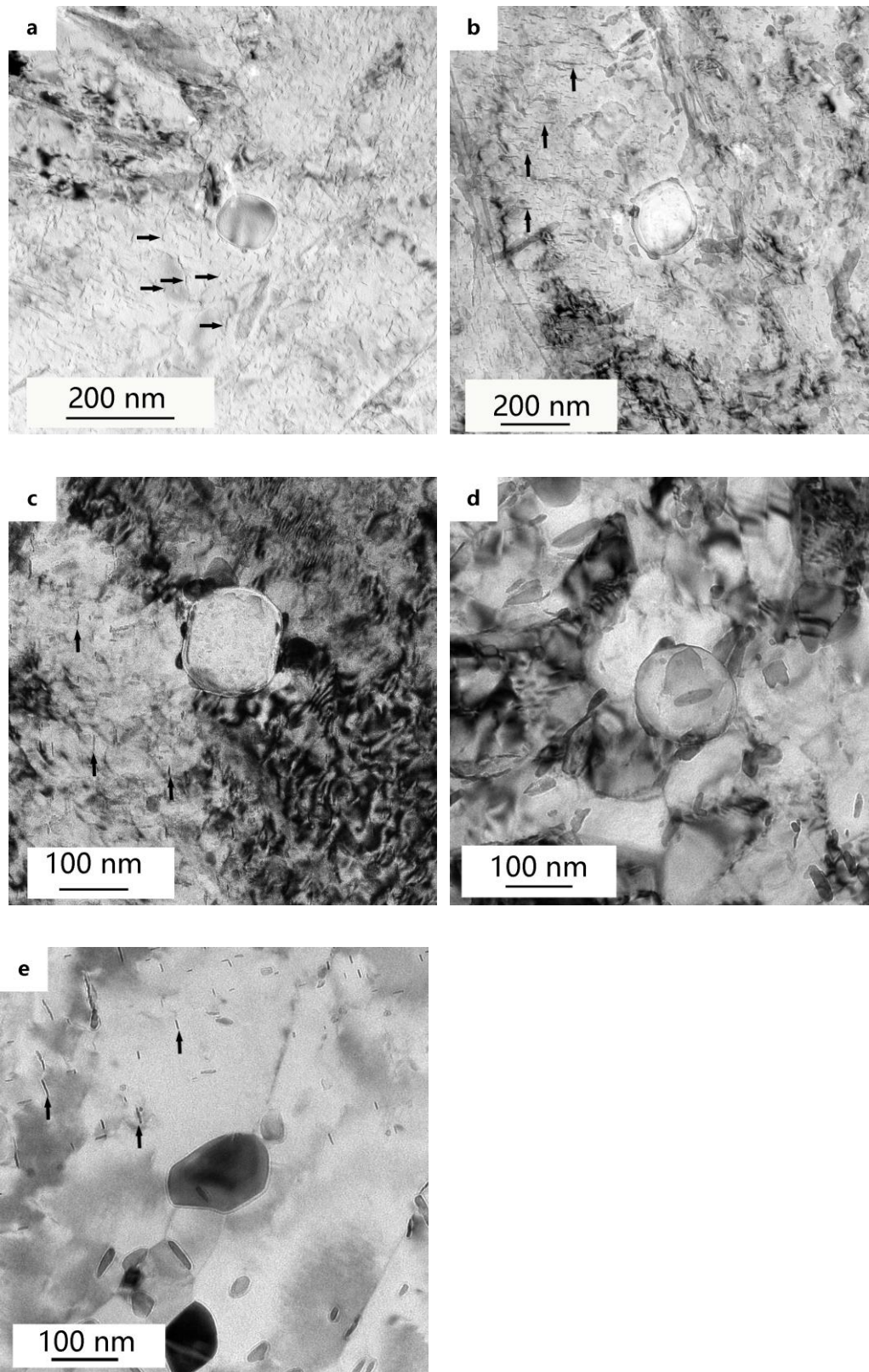
Figure 5. TEM images showing the presence of larger spherical carbides, elliptical carbides and very tiny needle-shaped carbides within martensitic laths in different tempering conditions: (a) 550 ℃ for 4 h; (b) 550 ℃ for 24 h; (c) 600 ℃ for 4 h; (d) 600 ℃ for 16 h; (e) 650℃ for 4 h.

Precipitation of different types of alloy carbides leads to variations in carbide morphologies on tempering at 550 - 650 ℃. In order to consistently check the substitutional element contents in carbides experimentally, the substitutional element M (M=Cr, Mo, V) to Fe ratio Y_M is used as defined in Equation (1)

$$Y_M = wt(M)/wt(Fe) \tag{1}$$

Where wt (M) and wt (Fe) are the weight percentages of M and Fe respectively from the EDS measurements. Firstly, spherical carbides have been ascertained as V-rich M_8C_7 carbides, Figure 6 (a) - (c), which are also supposed to be primary carbides, being consistent with those in the as-quenched microstructure in Figure 2 and 3. As listed in Table 2, spherical M_8C_7 carbides persist in all tempering conditions. Mo and Cr diffuse and segregate into M_8C_7 particles, Figure 6 (c) and Table 3, where Mo is the second predominating substitutional element constituting V-rich M_8C_7 particles, which roughly agrees with the thermodynamic prediction of equilibrium alloying contents in MC ranking as V > Mo > Cr. Secondly, very tiny needle-shaped carbides present within matrix, whose average length is much smaller than that of auto-tempered carbides in Figure 7, have been ascertained to M_2C carbides based on the HRTEM analysis in Figure 8. The transformation from auto-tempered carbides to M_2C in the ferritic matrix takes place for a short tempering time 4 h at 550 - 650 ℃, as shown in Figure 5, Table 2 and Figure 7. Tiny needle-like M_2C carbides are thermodynamically unstable at higher temperatures[2, 9], and easily coarsen and decompose to other alloy carbides as the number density decreases meaningfully with the increase of tempering temperatures for the constant tempering time 4 h, Figure 7. However, they can remain at relatively lower temperatures, like 550 ℃, for an extended tempering process (e.g. 24 h), Table 2 and Figure 5, resulting in a comparatively larger low-temperature tempering resistance for Dievar steel. Thirdly, small elliptical Cr-rich M_7C_3 carbides with an average length of 100 - 150 nm, Figure 6 (d) - (f), have been detected except for the tempering condition at 600 ℃ for 4 h, Table 2. As shown in Figure 9 (a) - (d), Cr have commenced to segregate along the boundaries to support the formation of Cr-rich carbides for a short tempering time (4 h) at 600 ℃[16]. The enrichment and redistribution of Cr in pre-existing particles (i.e. larger spherical V-rich M_8C_7 carbides) also gives the priority for Cr-rich carbides to nucleate at the interface of pre-existing carbides[23]. Additionally, larger elliptical Cr-rich $M_{23}C_6$ carbides with an average length of 150 - 200 nm appear at relatively

higher tempering temperatures or for a longer tempering time, Figure 6 (g) - (i) and Table 2, which are also calculated as one of equilibrium carbides in Dievar steel. As listed in Table 3, the higher Cr content in carbides in Figure 6 (i) demonstrates that more Cr segregates in Cr-rich particles, which is expected to promote the *in-situ* transformation of M_7C_3 to $M_{23}C_6$. Moreover, elliptical Mo-rich M_6C carbides with an average length of 200 - 250 nm, another simulated equilibrium carbide in this steel, have also been found on tempering at 550 - 600 ºC for 24 h, which concurrently exist with V-rich M_8C_7 and Cr-rich M_7C_3 and $M_{23}C_6$ carbides. As seen in Figure 9 (e) - (h), elliptical Cr, Mo-rich particles are distributed either around the primary V-rich carbides or along boundaries on tempering at 600 ºC for 24 h, which illustrates the coincidence of the *in-situ* transformation and separate nucleation and growth for secondary alloy carbides (like M_7C_3, $M_{23}C_6$ or M_6C) on tempering.
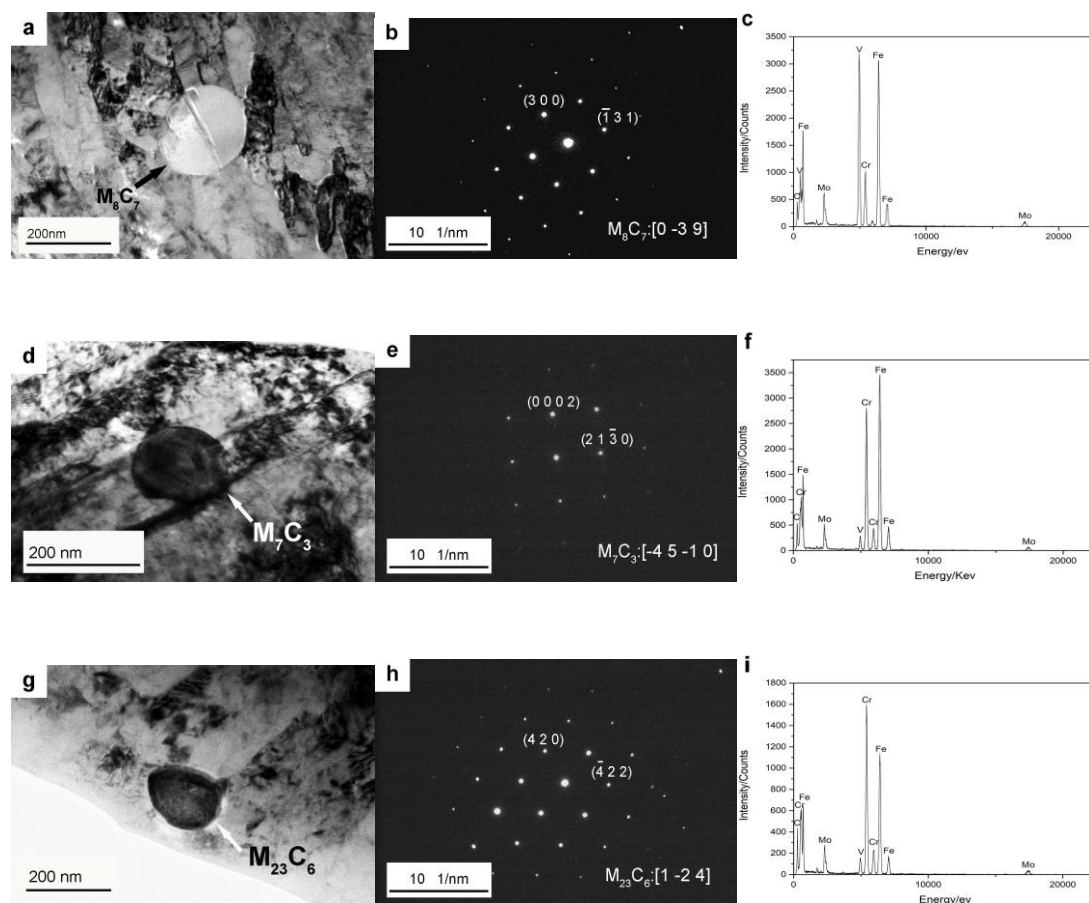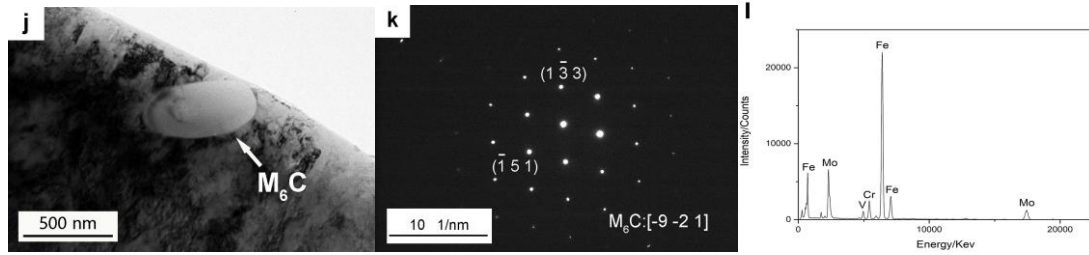
Figure 6. TEM images of different alloy carbides: (a) morphology of M_8C_7 carbide; (b) corresponding SAD pattern for the particle in (a); (c)EDX spectra for the spherical carbide in (a); (d) morphology of M_7C_3 carbide; (e) corresponding SAD pattern for the particle in (d); (f) EDX spectra for the elliptical carbide in (d); (g) morphology of $M_{23}C_6$ carbide; (h) corresponding SAD pattern for the particle in (g); (i) EDX spectra for the faceted carbide in (g); (j) morphology of M_6C carbide; (k) corresponding SAD pattern for the particle in (j); (l) EDX spectra for the carbide in (j).

Table 2. Summary of carbides identified in Dievar steel tempered at 550 / 600 / 650 ℃

Tempering temperature / ℃	Tempering time / h	Identified carbides				
		M_8C_7	M_2C	M_7C_3	$M_{23}C_6$	M_6C
	4	√	√			
550	16	√	√			
	24	√	√	√	√	√
	4	√	√	√		
600	16	√		√	√	
	24	√		√	√	√
	4	√	√	√	√	
650	16	√		√	√	
	24	√		√	√	√
Equilibrium carbides (Thermo-Calc calculation)		√			√	√

Table 3. The M to Fe ratio Y_M (M=Cr, Mo and V) for different carbides in Figure 6 from the EDS measurements on tempering

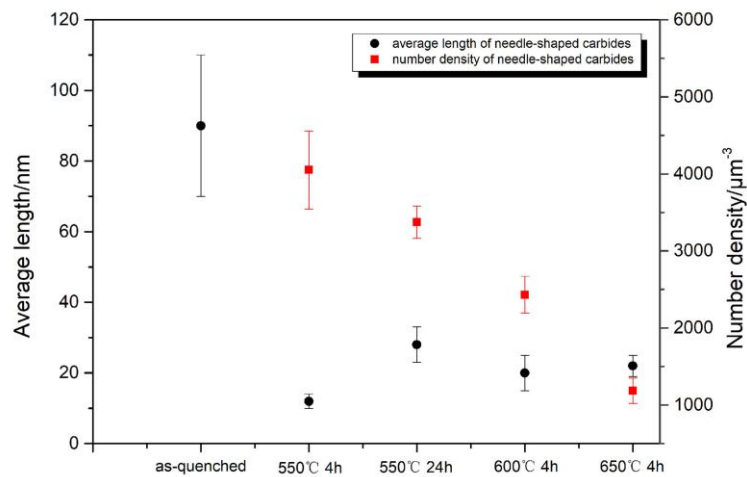|	Y_{Cr}	Y_{Mo}	Y_V
The spherical carbide in (a)	0.16±0.01	0.25±0.01	0.86±0.02
The elliptical carbide in (d)	0.69±0.02	0.16±0.01	0.06±0.01
The elliptical carbide in (g)	1.19±0.04	0.31±0.01	0.10±0.01
The elliptical carbide in (j)	0.08±0.01	0.53±0.02	0.06±0.01

Figure 7. The average length and number density variations for tiny needle-shaped carbides within martensitic laths on tempering.

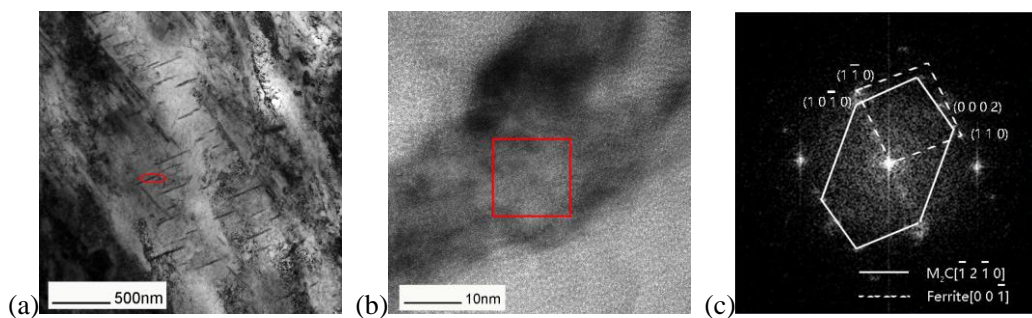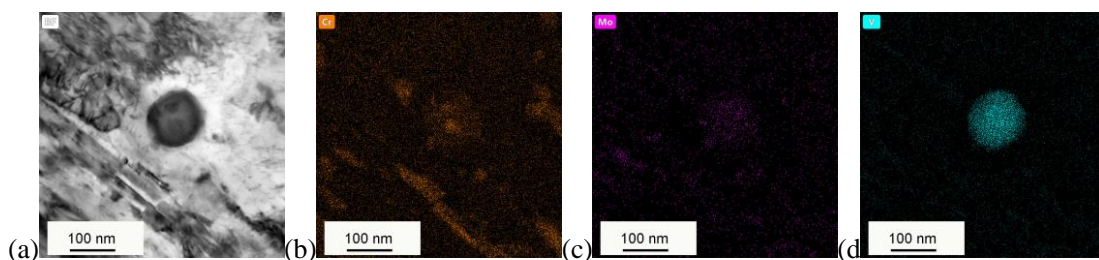

Figure 8. Confirmation of the type of needle-shaped carbides on tempering at 550 ℃: (a) the bright field image of a chosen area; (b) the HRTEM image of a selected carbide in (a); (c) FFT analysis of the selected carbide in (b).
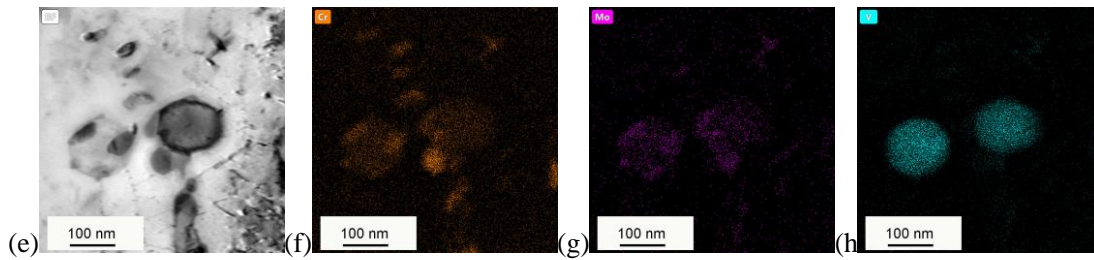
Figure 9. STEM EDS-mapping on different carbides precipitated in Dievar steel on tempering at 600 ℃ for 4 h: (a) the bright-field image showing the existence of spherical and smaller elliptical carbides; (b) - (d) elemental mapping; for 24 h: (e) the bright-field image showing the presence of spherical and elliptical carbides; (f) - (h) elemental mapping.

The boundary and matrix carbides in Figure 4 both coarsen and spheroidize during tempering, where larger carbides grow at the expense of smaller ones due to *Ostwald* ripening. Figure 10 shows the variations of carbide size and number density for inter- and intra-lath particles on tempering at 550 - 650 ℃. The sizes for the boundary carbides are larger than those for the matrix carbides due to the faster solute boundary diffusion. It has been shown that the coarsening rate for the boundary carbides varies noticeably with increasing tempering temperatures, e.g. from 550 to 650 ℃, Figure 10 (a) (b). The size of the boundary carbides rises mildly during tempering at 600 / 650 ℃ for a short tempering time, however, it climbs drastically on tempering at the same temperature for a long tempering time (i.e. 16 and 24 h), which can be seen in Figure 11. Nevertheless, the size for the matrix carbide keeps constant with increasing tempering temperatures, Figure 10 (a) (b), probably due to the newly-precipitated small alloy carbides replacing the previous larger pre-existing matrix particles. In addition, carbide number density decreases with tempering time due to the occurrence of carbide coarsening, Figure 10 (c).
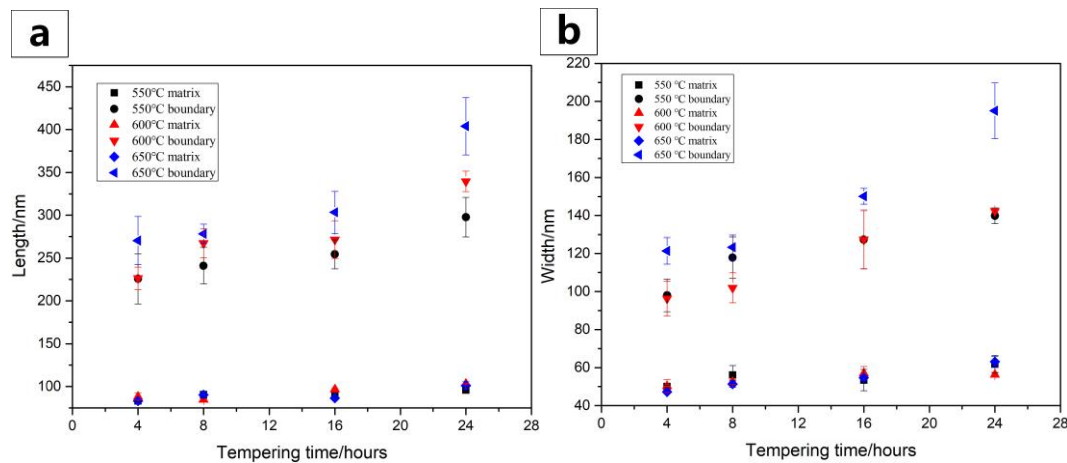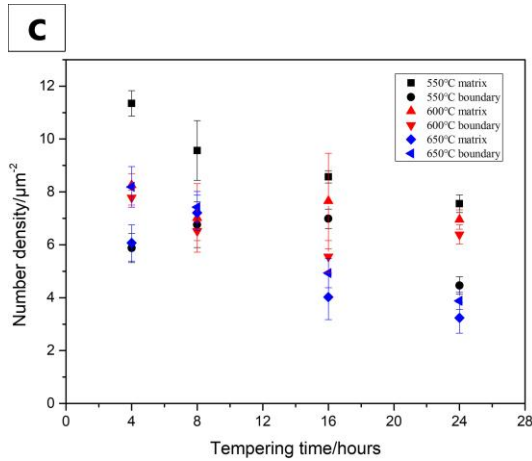
Figure 10. The average (a) length (b) width and (c) number density variations for carbides in Dievar steel in different tempering conditions.

3.3 Hardness variation on tempering

Figure 11 shows the hardness variation for Dievar steel in different tempering conditions, where the as-quenched hardness is approximately 55 HRC. It can be seen that the hardness remains at a high level (≥ 50 HRC) for tempering at 550 ℃, where no obvious hardness decrease takes place even for a long tempering time up to 24 h, giving Dievar steel a higher thermal stability at this temperature. However, the hardness decreases gradually from approximately 42 HRC to 31 HRC on tempering at 600 ℃ with the extension of time from 4 h to 24 h. Furthermore, with the increase of tempering temperatures from 600 ℃ to 650 ℃, the hardness decrease for the 4 h tempering condition is more obvious (41 HRC at 600 ℃ to 29 HRC at 650 ℃). Finally, the hardness decreases to 22 HRC for tempering at 650 ℃ for 24 h, which cannot meet the service requirements of this grade of steel.
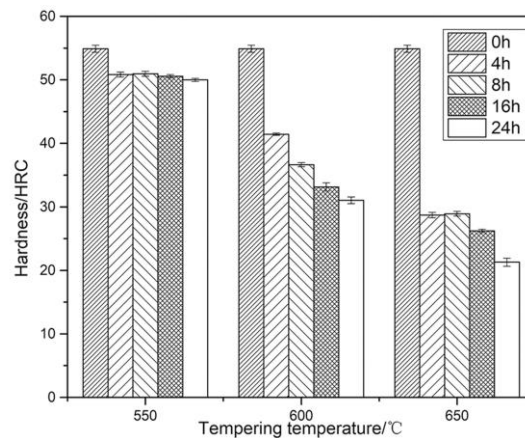

Figure 11. The hardness variation for Dievar steel after tempering at different temperatures.

4. Discussions

4.1 Carbide precipitation on quenching and tempering

As listed in Table 2, thermodynamically calculated equilibrium carbides in Dievar are V-rich MC, Cr-rich $M_{23}C_6$ and Mo-rich M_6C, which are slightly different from the identified carbides on quenching and tempering. The presence of V-rich primary carbides can pin the prior austenite grain growth to further refine the martensitic structure on quenching[23]. Lower bainite forms during oil quenching in Dievar with carbon diffusion under the para-equilibrium condition, where bainitic carbides, which are supposed to be cementite based on the observation in a X37CrMoV5-1 steel[24], appear as parallel arrays at about 60º to the axis of the bainitic plate due to its precipitation in one variant of the orientation relationship[25]. Lath martensite are present with auto-tempered carbides existing nearly in Widmanstätten arrays. Ms for Dievar approaches 328 ºC (JMatPro calculation), thus, carbon still has a certain diffusion ability below Ms (i.e. $D_{C-\alpha}$ (300 ºC) $=3.16\times10^{-14}$ m^2/s[26]) to segregate on dislocations to form carbides withins laths after martensite transforms.

It has been found that the carbide coarsening rate is associated with the diffusion of the rate-controlling alloying elements, such as Cr, Mn and V with a much lower diffusion coefficient compared to C[12, 14, 15]. Large spherical V-rich M_8C_7 carbides are left over from primary carbides and retained on oil quenching and tempering, however, coarsening of M_8C_7 occurs relatively sluggishly on tempering due to the slow diffusivity of V (e.g. $D_{V-\alpha(600ºC)}=1.4744\times10^{-14}$ m^2/s[27]). Cr and Mo segregate in the V-rich carbide interior, seen in Figure 3 (d) and Figure 6 (c), which prefer to distributed around primary carbide - ferrite interfaces[28-29]. The M_8C_7 carbide - ferrite interfaces with the enrichment of Mo and Cr can act as Cr / Mo sinks, giving rise to the heterogeneous nucleation for subsequent alloy carbides formed upon tempering, as shown in Figure 9. It has been reported that Mo-rich M_2C carbides precipitate after the formation of cementite in Cr-Mo-V steels with a high bulk Mo/V ratio during the early stage of tempering[30, 31]. M_2C carbides, keeping coherent with the ferritic matrix, start to precipitate as tiny needle-shaped particles with the aspect ratio of 1.0 - 4.0 in Dievar for a short tempering process, Figure 8, and grow in three equivalent

directions in Figure 5. These needle-shaped carbides remain stable at low temperatures even for an extended tempering procedure (i.e. at 550 ℃ for 24 h), Table 2. In addition, the formation of Cr-rich elliptical M_7C_3 carbides is much earlier compared to the other Cr-rich equilibrium $M_{23}C_6$ carbides in this steel for tempering at 600 ℃. Dislocations, distinct interfaces and grain / subgrain boundaries are regarded as active initiators for these carbides with low Gibbs energy barriers. Cr-rich carbides undergoes a gradual transition from M_7C_3 to $M_{23}C_6$ crystal structures based on the polymorphic transition mechanism in metals[32]. Y_{Cr} in Cr-rich carbides is gradually achieving the equilibrium value of 1.53 with prolonged tempering time, listed in Table 3. In high Cr-Mo containing steels[16, 33], the precipitation sequences for Cr-rich carbides have been established as cementite→M_7C_3→$M_{23}C_6$ or cementite→$M_{23}C_6$. Hence, it is expected that stable $M_{23}C_6$ carbides with a higher Y_{Cr} are reinforced in a long tempering schedule compared to M_7C_3 carbides in this steel. In addition, stable Mo-rich M_6C particles with an elliptical shape form at 550 - 600 ℃ for 24 h with the decomposition of metastable Mo-rich M_2C carbides, Table 2. These elliptical Cr-rich and Mo-rich carbides prefer to precipitate either via the *in-situ* transformation from pre-existing carbides (such as spherical V-rich M_8C_7) or by the separate nucleation along boundaries. As seen in Table 2, M_2C and M_8C_7 persist at lower tempering temperature of 550 ℃ for up to 24 h, whereas M_7C_3, $M_{23}C_6$ and M_6C are observed for a longer time of 24 h at the same temperature. A higher tempering temperature accelerates the carbide evolution process[6, 10]. M_2C carbides have only been observed on tempering at 600 / 650 ℃ for 4 h, which eager to transform to other stable alloy carbides[9]. M_8C_7, M_7C_3 and $M_{23}C_6$ have all been observed on tempering at 650 ℃ for 4 - 16 h. Therefore, based on the identification of alloy carbides, the precipitation sequence for this grade of steel can be addressed on oil quenching and tempering as followed: M_8C_7 + banitic carbides + auto-tempered carbides ➔ M_8C_7 + M_2C + M_7C_3 ➔ M_8C_7 + M_2C + M_7C_3 + $M_{23}C_6$ →M_8C_7 + M_7C_3 + $M_{23}C_6$ ➔ M_8C_7 + M_7C_3 + $M_{23}C_6$ + M_6C, which elucidates the progressive carbide transformation from pseudo-equilibrium particles to equilibrium ones for tempering.

4.2 The influence of carbide evolutions on hardness variations for tempering

As shown in Figure 11, the hardness remains at a high level ($\geqslant$ 50 HRC) for tempering at 550°C, where a large number of fine needle-shaped M_2C carbides present within the ferritic matrix giving a secondary hardening effect, Figure 5. The high number densities of needle-like M_2C particles at 550 ℃ for the 4 - 24 h tempering conditions in Figure 7 indicate that M_2C carbides can effectively and efficiently pin dislocation motions. As the average length for M_2C carbides increases from 10 to 40 nm on tempering from 4 h to 24 h at 550 ℃, the bypass strengthening mechanism plays the main role in the precipitation strengthening[34]. In addition, needle-shaped M_2C carbides are unstable and tend to transform to other equilibrium carbides at higher temperatures[2, 9, 30, 31], where the number density decreases significantly at 600 / 650 ℃, being consistent with hardness variations at the same temperature. Furthermore, coarsening of carbides also leads to the loss of coherency with the ferritic matrix, and a continuous hardness decrease occurs consequently. The rates of coarsening for carbides after tempering at 600 and 650 ℃ from 4 h to 24 h are much higher than that after tempering at 550 ℃ due to the faster diffusion of substitutional alloying elements at higher temperatures (i.e. $D_{Mo-\alpha}$(550 ℃)=3.7944$\times$ 10^{-15} m^2/s compared with $D_{Mo-\alpha}$(600 ℃)=1.2694$\times10^{-14}$ m^2/s, $D_{Mo-\alpha}$(650 ℃)=1.427$\times10^{-13}$ m^2/s[35, 36]). The estimated hardness values based on the Hírsch and Humphreys precipitation hardening equation[37, 38] at 550 ℃ in Figure 12 sustains the highest ($\geqslant$ 320 HB) compared to other tempering conditions at 600 and 650 ℃, which agrees with the practical hardness results in Figure 11. A comparatively slower coarsening rate at 550 ℃ results in a lower hardness decrease (44 HB) compared to that at 600 ℃ (110 HB). Moreover, there is a consecutive hardness decrease (practical and estimated) at 600 ℃ in Figure 11 and 12, which is derived from the continuous growth of carbides and consistent with the carbide size variation in Figure 10. Finally, the hardness values at 650 ℃ remain the lowest due to the presence of larger particles, where the precipitation hardening contribution between 4 h and 16 h tempering conditions at 650 ℃ exhibits almost no difference, being consistent with the carbide size variation in Figure 10 and practical hardness values in Figure 11.
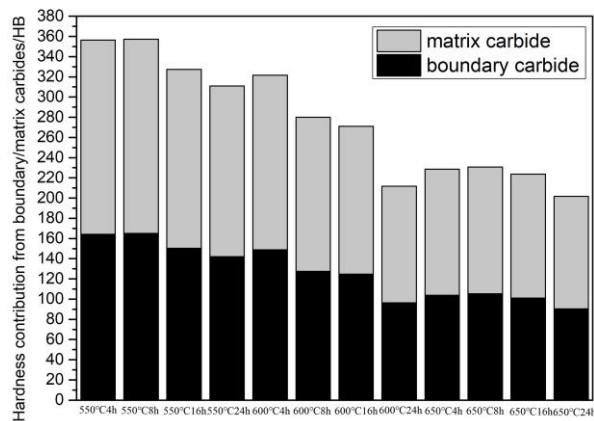
Figure 12. Predicted (using Hírsch and Humphreys precipitation hardening equation) boundary/matrix carbide contribution to hardness in Dievar steel after tempering for 4 h, 8 h, 16 h and 24 h at 500 / 600 / 650 ℃.

5. Conclusion

Carbide precipitation and coarsening behaviors related with hardness variations in Dievar steel have been quantified and characterized in detail, where the effect of alloying elements Cr, Mo and V has been considered. The main conclusions are:

(1) The precipitation sequence for Dievar steel can be addressed on oil quenching and tempering as followed: M_8C_7 (V-rich) + banitic carbides + auto-tempered carbides → M_8C_7 + M_2C (Mo-rich) + M_7C_3 (Cr-rich) → M_8C_7 + M_7C_3 + $M_{23}C_6$ (Cr-rich) → M_8C_7 + M_7C_3 + $M_{23}C_6$ + M_6C (Mo-rich).

(2) Carbides coarsen on tempering, where the sizes for boundary carbides are obviously larger than those for matrix carbides due to the faster solute lath/grain boundary diffusion. The sizes for boundary carbides increase noticeably with increasing tempering temperatures, e.g. from 600 ℃ to 650 ℃, whereas the sizes for matrix carbides nearly keep constant.

(3) The hardness remains at higher than 50 HRC on tempering at 550 ℃ even for 24 h probably due to a fine dispersion of needle-shaped M_2C carbides within laths to pin dislocation motions. However, the hardness drops rapidly for tempering at 600 and 650 ℃ because of the gradual dissolution of unstable needle-shaped carbides and the coarsening of elliptical alloy carbides, like Cr-rich $M_{23}C_6$ and M_7C_3.

Data availability

The raw/processed data required to reproduce these findings cannot be shared at this time due to legal or ethical reasons.

References

[1] Gopalsamy B M, Mondal B, Ghosh S, et al. Experimental investigations while hard machining of DIEVAR tool steel (50 HRC). Int J Adv Manuf Technol, 2010, 51 (9-12): 853-869. https://doi.org/10.1007/s00170-010-2688-1 .

[2] Rong W and Dunlop G. The crystallography of secondary carbide precipitation in high speed steel. Acta Metallurgica, 1984, 32: 1591. https://doi.org/10.1016/0001-6160(84)90218-9 .

[3] Mesquita R A, Barbosa C A, Machado A R. Heat Treatment of Tool Steels. Comprehensive Materials Finishing, 2 (2016), 214. https://doi.org/10.1016/B978-0-12-803581-8.09191-8

[4] Jesperson H. Influence of the heat treatment on the toughness of some hot-work tool steel grades. La Metallurgia Italiana, 2013, XCIII(2): pp. 29-37.

[5] Zhou J, Ma D, Chi H, et al. Microstructure and properties of hot working die steel H13MOD. J. Iron Steel Res. Int, 2013, 20 (9): 117-125. https://doi.org/CNKI:SUN:YING.0.2013-09-019 .

[6] Song W, Min Y, Wu X. Study on carbides and their evolution in H13 hot work steel. Trans. Mater. Heat Treat. 2009, 30, 122-126. https://doi.org/10.1016/j.elecom.2008.10.019

[7] Mebarki N, Delagnes D, Lamesle P,et al. Relationship between microstructure and

mechanical properties of a 5% Cr tempered martensitic tool steel. Mater Sci Eng A-Struct Mater Prop Microstruct Process. 2004, 387-389: 171-175. https://doi.org/10.1016/j.msea.2004.02.073

[8] Wang H, Li J, Shi C B, et al. Evolution of Carbides in H13 Steel in Heat Treatment Process[J]. Materials Transactions, 2017, 58(2):152-156. https://doi.org/10.2320/matertrans.M2016268

[9] Zhang Z, Zhang J, Yao Z, et al. Design for novel hot-work die steel by thermodynamic calculation and microstructural examination. Metals. 2019, 9 (805): 1-13. https://doi.org/10.3390/met9070805

[10] Zhang Z, Delagnes D, Bernhart G. Microstructure evolution of hot-work tool steels during tempering and definition of a kinetic law based on hardness measurements. Mater Sci Eng A-Struct Mater Prop Microstruct Process, 2004, 380 (1/2): 222-230. https://doi.org/10.1016/j.msea.2004.03.067 .

[11] Mellouli D, Haddar N, Koster A, et al. Thermal fatigue failure of brass die-casting dies. Eng Fail Anal, 2012, 20 (3): 137-146. https://doi.org/10.1016/j.engfailanal.2011.11.006 .

[12] Li T S, Wang F M, Li C R, et al. Carbide Evolution in High Molybdenum Nb-microalloyed H13 Steel during Annealing Process. J Iron Steel Res, 2015(4):7. https://doi.org/10.1016/S1006-706X(15)30008-X

[13] Delagnes D, Lamesle P, Mathon M H, et al. Influence of silicon content on the precipitation of secondary carbides and fatigue properties of a 5% Cr tempered martensitic steel. Mater Sci Eng A-Struct Mater Prop Microstruct Process. 2005, 394: 435-444. https://doi.org/10.1016/j.msea.2004.11.050

[14] Clarke K D, Van-Tyne C J, Vigil C J, et al. Induction hardening 5150 steel: Effects of initial microstructure and heating rate. J Mater Eng Perform. 2011, 20, 161-168. https://doi.org/10.1007/s11665-010-9825-8

[15] Sadhan G. Rate-controlling parameters in the coarsening kinetics of cementite in Fe-0.6C steels during tempering. Scr. Mater. 2010, 63, 273-276. https://doi.org/10.1016/j.scriptamat.2010.04.002

[16] Inoue A, Masumoto T. Carbide reactions (M3C→M7C3→M23C6→M6C) during tempering of rapidly solidified high carbon Cr-W and Cr-Mo steels. Metall Mater Trans A. 1980, 11A: 739-747. https://doi.org/10.1007/BF02661203

[17] Kuo K, Jia C. Crystallography of M23C6 and M6C precipitated in a low alloy

steel. Acta Metall. 1985, 33 (6): 991-996. https://doi.org/10.1016/0001-6160(85)90193-2

[18] Xia S, Zuo P, Zeng Y, et al. Influence of nickel on secondary hardening of a modified AISI H13 hot work die steel. Materialwiss Werkstofftech, 2019, 50 (2):197-203. https://doi.org/10.1002/mawe.201700205

[19] Lin Y, Zheng Y, Wu Z , et al. A discussion of the effects of composition and heat treatment on the toughness of a medium carbon secondary hardening steel. Mater Sci Eng A-Struct Mater Prop Microstruct Process. 2019, 748: 213-227. https://doi.org/10.1016/j.msea.2019.01.079

[20] Ferrari M T C, Andersson J, Kvarnström M. Influence of lowered austenitisation temperature during hardening on tempering resistance of modified H13 tool steel (Uddeholm Dievar). International Heat Treatment and Surface Engineering. 2013, 7 (3): 129-132. https://doi.org/10.1179/1749514813Z.00000000071

[21] Chen R, Wang Z, Qi L, L.et al. The carbides, tensile properties, and work hardening behavior of annealed H13 die steels with varied yttrium contents. Mater Sci Eng A-Struct Mater Prop Microstruct Process. 2021, 806, 140856: 1-10. https://doi.org/10.1016/j.msea.2021.140856

[22] Rao K, Prabhu K N. A Comparative Study on Cooling Performance of Hot Oil and Molten Salt Quench Media for Industrial Heat Treatment. J. Mater. Eng. Perform., 2020, 29(6): 3494–3501. https://doi.org/10.1007/s11665-020-04635-x .

[23] Shi K F, Zhao F, Liu Y, Yin S and Yang R G. The Effect of the pre-existing VC on the evolution of precipitate and mechanical properties in the H13 steel. Materials. 2022, 15, 3970.

[24] Mayer S, Scheu C, Leitner H, etal. Correlation between heat treatment, microstructure and mechanical properties of a hot-work tool steel. Int J Mater Res, 2009, 100(1):86-91. https://doi.org/10.3139/146.101782

[25] Bhadeshia H K , Honeycombe S R. Steels: Microstructure and Properties. Oxford (UK): Butterworth-Heinemann Press, 2017.

[26] Gamsjäger E, Svoboda J, Fischer F D. Austenite-to-ferrite transformation in low-alloyed sreels. Comput Mater Sci. 2005, 32, 360. https://doi.org/10.1016/j.commatsci.2004.09.031

[27] Ju Y, Goodall A, Strangwood M, Davis C. Characterisation of precipitation and carbide coarsening in low carbon low alloy Q&T steels during the early stages of tempering. Mater Sci Eng A-Struct Mater Prop Microstruct Process. 2018, 738:

174-189. https://doi.org/10.1016/j.msea.2018.09.044

[28] Tomita Y, Okabayashi K. Mechanical properties of 0.4C-Ni-Cr-Mo high strength steel having a mixed structure of martensite and bainite. Metallurgical Transactions A, 1985(7316A): 73. https://doi.org/10.1007/BF02656714

[29] Cabrol E, Bellot C, Lamesle P, et al, Experimental investigation and thermodynamic modeling of molybdenum and vanadium-containing carbide hardened iron-based alloys. J Alloy Compd. 2013, 556: 203. https://doi.org/10.1016/j.jallcom.2012.12.119

[30] Bowen A W, Leak G M. Diffusion in Bcc iron base alloys. Metall Mater Trans B-Proc Metall Mater Proc Sci. 1970, 1, 2767-2773. https://doi.org/10.1007/BF03037813

[31] Výrostková A, Kroupa A, Janovec J, et al. Carbide reactions and phase equilibria in low alloy Cr-Mo-V steels tempered at 773-993 K. Part I: Experimental measurements. Part I: Experimental measurements. Acta Mater. 1998, 46, 31-38. https://doi.org/10.1016/S1359-6454(97)00238-3

[32] Kraposhin V S, Yu S, Talis A L, et al. Experimental investigation of in-situ transformations of the M7C3 carbide in the cast Fe-Cr-Ni alloy. Phys Metals Metallogr. 2017, 118, 233. https://doi.org/10.1134/S0031918X17030097

[33] Thomson R C, Bhadeshia H K D H. Carbide precipitation in 12Cr1MoV power plant steel. Metall Mater Trans A. 1992, 23, 1171-1179. https://doi.org/10.1007/BF02665048

[34] Fu J , Li G , Mao X , et al. Nanoscale cementite precipitates and comprehensive strengthening mechanism of steel. Metall. Mater. Trans. A 2011, 42A, 3797–3812. https://doi.org/10.1016/S1872-2040(10)60412-4

[35] Kucera J, Million B, Ciha K. Diffusion of Mo,W and V in Fe-Cr Alloy with BCC Lattice. Kov Mater. 1969,7: 97-107. https://doi.org/10.1103/PhysRev.109.605 .

[36] Bowen A W, Leak G M. Solute Diffusion in α and γ Iron. Met Trans. 1971:1695. https://doi.org/10.1007/BF02642019 .

[37] Shewmon P G. Diffusion in Solids, second ed, McGraw-Hill, 1963. https://doi.org/10.1007/978-3-319-48206-4 .

[38] Hírsch P B, Humphreys F J, Plastic deformation of two-phase alloys containing small nondeformable particles. Physics of strength and plasticity, MIT Press, Cambridge, 1969.